Batteries & Supercaps

Research Article
doi.org/10.1002/batt.202400768

Chemistry Europe
European Chemical Societies Publishing

www.batteries-supercaps.org

High Shear Dispersion Techniques for Up-Scaling and Controllable Cathode Morphology in High Performance Li–S Pouch Cells

Ralf Schmidt,[a, b] Tom Boenke,[a] Paul Härtel,[a] Susanne Dörfler,*[a] Thomas Abendroth,[a] Holger Althues,[a] and Stefan Kaskel[a, b]

The lithium sulfur (Li–S) cell chemistry is promising due to the high specific capacity of its active materials resulting in high specific energy cells. In the past years, the number of publications on practical prototype cells have increased, already reporting high specific energies over 400 Wh kg^{-1} with low electrolyte-to-sulfur (E:S) ratios. To enable the complex conversion chemistry at low E:S ratios, the cathode porosity adaption is crucial and depends for example on the suspension blending procedure. There are several methods and devices to prepare suspensions for battery electrodes, e.g. dissolver and planetary mixers. In this study, a standard laboratory blender with low shear forces (EL1) is compared with a high shear mixer (HSM) for preparing porous carbon-sulfur suspensions in a relevant scale. In this study, the influence of the slurry preparation on the final performance is investigated by coating via slot die on a roll-to-roll device to produce carbon-sulfur-cathodes. The electrodes are characterized via optical and mechanical measurements. Electrochemical analysis is conducted using coin cells for pre-evaluation as well as multi-layered pouch cells with reduced electrolyte volume (3.0 µl mg-(S)$^{-1}$). It could be shown that the HSM enables increased binder dispersion and enhanced density leading to improved cycle life.

Introduction

Lithium-Sulfur (Li–S) batteries belong to the most promising energy storage technologies due to their usage of abundant and low-cost sulfur, which offers high theoretical capacity (1672 mAh g^{-1}) and, combined with a metallic lithium anode, the cells have a high theoretical specific energy (≈2600 Wh kg^{-1}).[1–4] For comparison, this value exceeds the state-of-the-art (SOTA) lithium ion batteries by factor five.[5] First prototype Li–S batteries with specific energies above 400 Wh kg^{-1} were already published.[6–8] Hence, this technology is notably suitable for lightweight applications such as aviation.[9,10] Furthermore, the preparation of cathodes do not require toxic and hazardous solvents and materials. However, it is still challenging to commercialize Li–S batteries due to issues such as the insufficient cycle life under practical conditions like low electrolyte-to-sulfur (E:S) ratios, high C-rates and high active material loadings. This drawback is caused by the highly reactive Li anode, which decomposes the electrolyte and grows dendritically leading to short circuits.[10] Another problem is the so-called polysulfide shuttle, which consumes active material and therefore leads to lower capacities.[2] This phenomenon especially takes place in SOTA ether-based electrolytes like 1,2-dimethoxyethane (DME)/1,3-dioxolane (DOL), which almost completely dissolve the sulfur and his conversion products allowing an easy migration to the Li anode. To overcome this hindering effects, several approaches have been reported so far such as electrolyte modifications,[11–13] carbon materials with reduced polysulfide shuttle[14–16] and protective lithium coatings or layers.[17–19] Regarding the cathode, various formulations and materials have been described, but parameters as the density were often not stated or taken into account. In 2015, a study reported only 31 out of 274 publications mentioned the thickness and sulfur load of the used cathodes.[20] Additionally, the impact of the cathode porosity has not been fully understood, yet. Gröbmeyer et al. and Li et al. communicated an increased capacity retention with densified carbon-sulfur (C–S) cathodes.[21,22] Titscher et al. showed that densified cathodes did not influence the electrochemical performance under C-rates of 1.0 C.[23,24] Kang et al. stated that compacting the cathode beyond a certain density leads to a reduced capacity.[25] All of these tests were run with DME/DOL. Schmidt et al. reported that densified cathodes lead to a decreased sulfur utilization in the first cycles when using DME/DOL electrolyte. The differences level out over cycling number. By implementing the sparingly polysulfide solvating electrolyte (SPSE) hexyl methyl ether (HME)/DOL, however, there was almost no impact on the cathode performance.[24] These contrary results originate through the use of different blending procedures, carbon hosts, cell types and E:S ratios making comparisons more difficult,

[a] R. Schmidt, T. Boenke, P. Härtel, S. Dörfler, T. Abendroth, H. Althues, S. Kaskel
Battery Technology, Fraunhofer Institute for Material and Beam Technology IWS, Winterbergstraße 28, 01277 Dresden, Germany
E-mail: Susanne.doerfler@iws.fraunhofer.de

[b] R. Schmidt, S. Kaskel
Chair of Inorganic Chemistry I, Technical University Dresden, 01069 Dresden, Germany

Supporting information for this article is available on the WWW under https://doi.org/10.1002/batt.202400768

Research Article
doi.org/10.1002/batt.202400768
Chemistry Europe
European Chemical Societies Publishing

though. Unfortunately, the results were mostly not obtained in pouch cells, but gained under flooded electrolyte regime leading to low projected energies. The usage of lean electrolyte amounts is crucial for Li–S batteries, though, because over 40% of the cell weight is contributed by the electrolyte.[10] For reaching higher gravimetric energy densities and,thus, practical relevance it is necessary to lower the weight contribution of all materials, which are not needed for the electrochemical reaction.[26] It is expected that cells being built under lean electrolyte conditions show a higher sensitivity to electrode porosity, as cathode swelling or increasing anode porosity could lead to a deficit of electrolyte and thus accelerating the cell failure. For Li–S batteries, small lab-scale processes with swing mills are common that are, however, difficult to scale up to larger cathode production as their maximum volume is limited and changing the process leads to differences in the applied shear forces, which are crucial to properly disperse binders and viscosity mediators in a suspension. Less is published on scaling up suspension-based manufacturing of sulfur cathodes for Li–S batteries.

In this study, the influence of the dispersion method for a water-based C–S-suspension on the cathode microstructure as well as electrochemical behavior of Li–S cells is evaluated. The aqueous slurries based on sulfur-melt-infiltrated porous carbon were mixed by using two blenders with different shear forces and then coated via a slot die on a roll-to-roll device to realize an up-scaled, application-oriented process without using toxic solvents. The produced cathodes were analyzed by using confocal and scanning electron microscopy (SEM) and electrochemical tests. In the latter case, coin cells were used to pre-evaluate the performance and in the second step, multi-layered pouch cells were built to gain practically relevant results regarding the electrolyte amount and cycle life. Therefore, the SOTA electrolyte DME/DOL and the SPSE HME/DOL were used to gain information about the relevance of the conversion chemistry regarding the lowered E:S ratio. It is shown that the dispersion of the suspension and as consequence the porosity of the electrode have a strong impact on the cycle life, which has to be taken into account to produce Li–S batteries for real applications in the future.

Results and Discussion

First, the mixing process is evaluated regarding viscosity, resulting cathode density and microstructure. Subsequently, the electrochemical performance in coin cells is pre-evaluated and transferred to multi-layered pouch cells then.

Mixing Process

After preparing the suspension, the coating and drying step were done in a concerted process, and the dispersion step mainly influences the resulting cathode morphology. For the investigation, all electrodes were generated by implementing 60% sulfur, 25% porous carbon black, 10% multi-walled carbon nanotubes (MWCNT) and 5% binder by weight with a targeted loading of 2.2 mg(S) cm^{-2}. The first dispersion strategy was conducted by using a relatively common laboratory mixer (Eirich, EL1). This mixing tool is characterized by a star-type rotor in the center of the vessel spinning with defined speed, while the vessel is rotating in the same direction. A knife fixed at the lid was dipping into the suspension for increased dispersion rate. This technique represents a methodology exerting comparatively low shear stress. For the second strategy, a high-shear mixer (Silverson, L5 M, HSM) was used. This blender was chosen as preliminary experiments with laboratory swing mill led to homogenous coatings via doctor blade technique, very likely due to the stark shear forces on the suspension generated by the steel spheres. The Silverson L5 M is equipped with an engine having a power of 250 W. The device is a high-shear lab mixer, suitable for volumes between 1 ml to 10 l. The blenders are illustrated in Figure 1. In general, higher shear stress is expected to lead to smaller particle sizes as it destroys agglomerated structures.

For validating both mixing strategies, their general behavior regarding process engineering was evaluated. To describe a dispersion process, characteristic numbers were established, which allow comparing different processes. One is the so-called Reynolds number Re. It helps predicting the flow patterns in a liquid system. $Re < 10^1$ describes a laminar flow, $Re > 10^4$ means a turbulent flow. Values in between belong to a transition zone. In general, turbulent flows promote a good dispersion of solids in a liquid phase.[27] Another relevant variable is the shear rate γ. It describes the applied shear strain to a material. For the manufactured suspensions, a pseudoplastic behavior was observed meaning the viscosity is decreased by increasing the shear rate. Considering this phenomenon is important, because for calculating Re the dynamic viscosity η of the suspension is necessary. For pseudoplastic media, the representative dynamic viscosity η_{rep} is used for calculating Re. For getting η_{rep}, the flow curve of the suspension has to be known. η_{rep} is read by taking the representative shear rate γ_{rep} for the process, which is calculated by the rotational frequency n of the stirrer and the Metzner-Otto constant k.[27] k is known for a lot of stirrer geometries. The results of the calculation for both blenders can be found in Table S1. It can be stated that the HSM creates a turbulent flow and the shear rate is more than 50 times higher

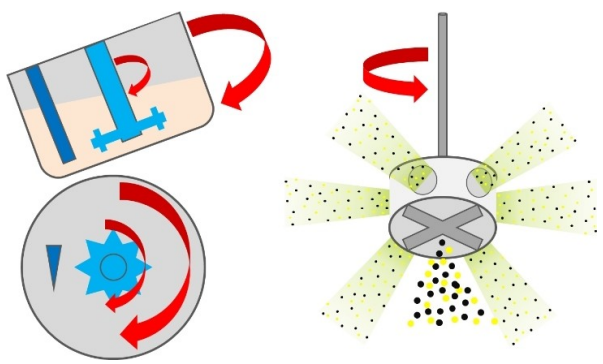

Figure 1. Schematic illustration of the laboratory mixer EL1 (left) and the high-shear mixer HSM (right).

Research Article
doi.org/10.1002/batt.202400768
Chemistry Europe
European Chemical Societies Publishing

compared to the EL1. These results allow classifying the HSM as the high shear stress and, for comparison, the EL1 as low shear stress blender.

Figure 2 shows the particle size distribution (PSD) of the pristine composite material (green), the HSM-suspension (black) and the EL1-suspension (red). The existence of agglomerates in the suspension prepared with EL1 can be seen, while the PSD of the HSM-suspension looks similar to those of the pristine material, as higher shear forces affect the dispersion of binder molecules. In order to further analyze the suspension, rotational viscosimetry was carried out and it was shown that the dynamic viscosity η of the HSM-suspension is lower compared to the EL1 as displayed in Table 1.

This difference could be caused by agglomerates leading to higher resistances while shearing the suspension. At higher shear rates, an assimilation of the dynamic viscosities is observable.

Consequently, the morphology of the HSM-electrode is changed to a less cracked surface, as can be seen in laser scanning microscopy (LSM) images in Figure S1. The reason is the homogeneous distribution of binder, which allows building up more connection points between the particles. The smaller particle size promotes this effect. Therefore, the surface roughness S_a as shown in Table 1 is decreased drastically, too. A smooth and homogeneous cathode surface is desired as it will cause less stress on metallic Li anode side while stripping/plating related to lower current density peaks. In addition, the density of the HSM-electrode is enhanced as shown in Table 1. Hg intrusion porosimetry was carried out to investigate the porosity of both cathodes. As illustrated in Figure S2, it could be shown that the porosity evoked by pores smaller than 1 μm is comparable, but pores above a size of 10 μm predominate in the EL1-cathode. This leads to the effect that the total pore volume is noticeably bigger, as shown in Table 1.

By analyzing the morphology imaged via SEM, the existence of bigger particles is observable for the EL1-electrode as shown in Figure 3b,c In comparison, the HSM-electrode shows only smaller particles and the absence of agglomerates as displayed in Figure 3f. After coating and drying, the mechanical behavior of the two electrodes was characterized by a tensile strength test. A reasonable adhesion on the current collector is beneficial for handling the electrodes and withstanding the volume expansion while discharge reaction takes place. The good dispersion of binder molecules in the HSM-electrode leads to an increase of the tensile force compared to EL1-electrode as displayed in Table 1. Additionally, the composite volume resistivity (CVR) was measured to reveal the influence of different blending procedures on the electrical conductivity of the coating. As already mentioned, the better dispersion of the HSM leads to an increased density, an absence of agglomerates and supports the homogeneous distribution of sulfur-infiltrated carbon particles, conductive additive and binder molecules. Therefore, the CVR of the HSM-electrode is reduced compared to the EL1-electrode. The increased conductivity of the HSM-electrode should promote the electrochemical performance.

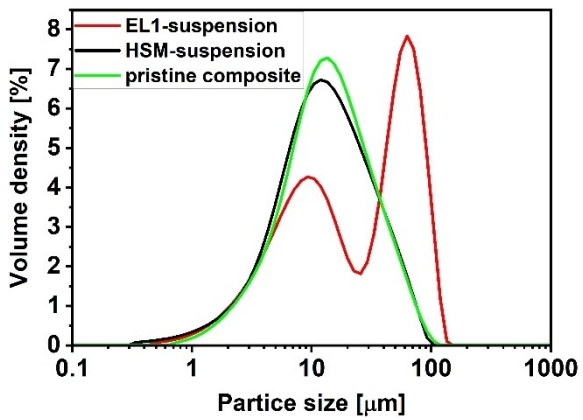

Figure 2. Particle size distribution of the composite material (green), the HSM suspension (black) and the EL1 suspension (red).

Electrochemical Performance in Coin Cells

To verify the influence of the electrode morphology, it was decided to use two different electrolyte systems basing on different conversion mechanism. DME/DOL as state-of-the-art electrolyte has a good ionic conductivity and polysulfide (PS) solubility. The general known conversion chemistry of Li–S batteries is described by using this electrolyte. The influence of the cathode density on the electrochemical performance using DME/DOL electrolyte is not fully understood because of contradicting results as mentioned in the introduction. The addition of $LiNO_3$ is necessary to support the solid electrolyte interphase

Table 1. Characteristics of HSM- and EL1-suspension/electrode.

	EL1-blender	HSM-blender
Cathode density in g cm^{-3}	0.35	0.50
Dynamic Viscosity @ 10 s^{-1} in mPa s	670	330
Dynamic Viscosity @ 100 s^{-1} in mPa s	280	230
Composite Volume Resistivity in Ohm cm	0.78	0.48
Tensile Force in Pa	7.5	14.7
Surface Roughness S_a in μm*	21.9	3.8
Total pore volume in cm^3 g^{-1}(coat.)	2.85	1.87

*calculated by analyzing the images shown in Figure S2.

Research Article
doi.org/10.1002/batt.202400768
Chemistry Europe
European Chemical Societies Publishing

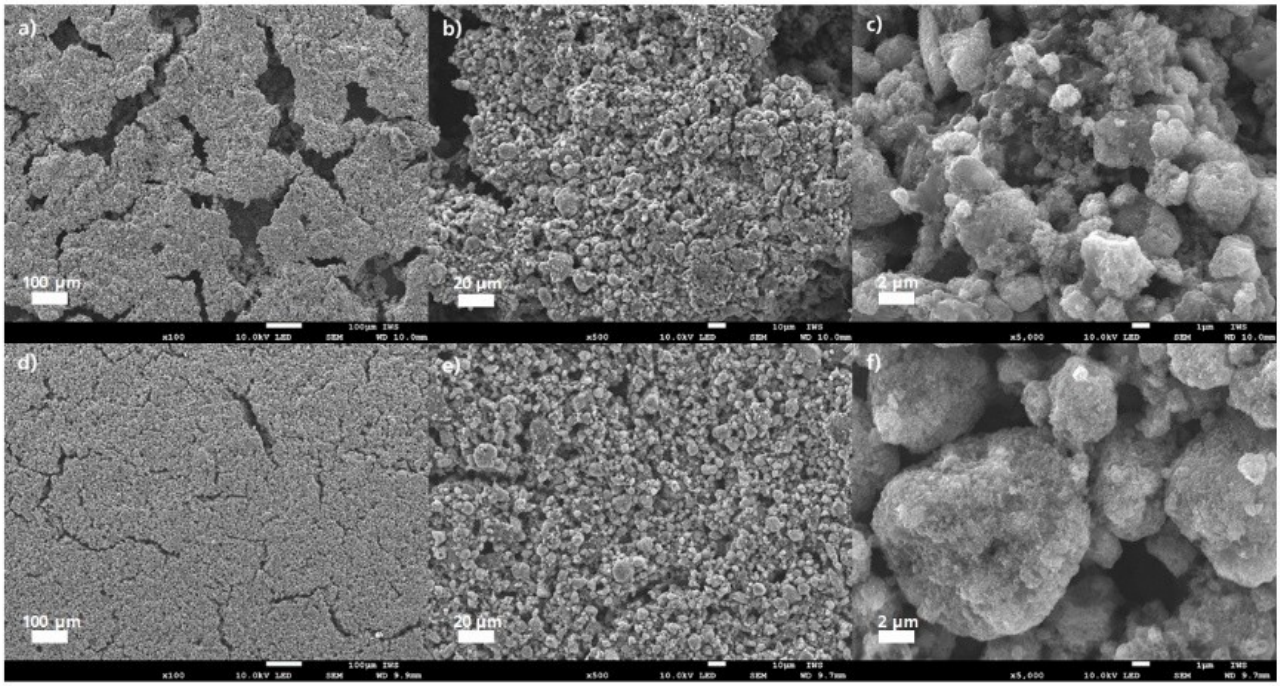

Figure 3. SEM images of the EL1-electrode (a–c) and the HSM-electrode (d–f) with magnifications from 100× (left) to 5000× (right).

(SEI) formation and thus increasing the cycle life of the cell.[28,29] It also catalyzes the oxidation of PS to elemental sulfur on cathode side.[30,31] An impact of this salt on the electrochemical behavior of the cathodes with different porosities is not expected. HME/DOL as SPSE was chosen to investigate the different blender effects also for an electrolyte system with alternative conversion chemistry, and to compare it with former studies on DRYtraec®-cathodes.[24] The coin cells were tested with an asymmetrical rate test meaning the charge current stayed constant, while the discharge current was varied over different intervals. This method allows gaining results related to the rate capability and cycle life at the same time. In the first testing campaign, both electrodes were run as prepared with DME/DOL electrolyte. The initial discharge capacity of the EL1-electrode was slightly higher than the HSM-electrode (1329 and 1280 mAh $g(S)^{-1}$). The difference refers to the smaller capacity after the first discharge plateau presumably caused by the higher density of the HSM-electrode. By lowering the porosity of the electrode, less electrolyte is available to dissolve the PS, leading to an increased PS concentration, which increases the transport resistances and therefore the sulfur utilization is decreased. This phenomenon was already reported by Schmidt et al.[32] and is observed for all C-rates as shown in Figure 4a. It is worth mentioning that the second discharge plateaus of both electrodes are on the same potential level meaning there are no additional resistances caused neither by the higher density nor by changes of the particle system induced by higher shear rates. As displayed in Figure 4b, the voltage dip of the HSM-electrode at 0.2 C is more pronounced referring to a higher resistance related to an increase in viscosity of the PS-saturated electrolyte in combination with a denser cathode.[33] At C-rates >0.2 C, this overpotential, caused by the viscosity increase and hence the higher resistances, leads to an undercut of the lower voltage window and thus the conversion reaction is limited.[33] Schmidt et al. and Kensy showed an assimilation of the capacity curves with different densities after a few cycles, which was induced by swelling of the cathodes after wetting.[24,34] To evaluate the behavior of the prepared electrodes after wetting, a similar test carried out by Schmidt et al.[24] with both electrolytes was done revealing no obvious swelling occurred as shown in the Figure S3. As result, the capacity differences remain over cycle life. This also means that the slurry-based cathodes have less intrinsic tension compared to the DRYtraec® ones. Very likely, during the liquid dispersion, all swellable compounds expand, whereas in the dryfilm coating without any solvent during processing, a certain residual stress within the cathode is retained.

In HME/DOL electrolyte, the conversion reaction behaves quasi solid-solid like.[11] As already discussed, Schmidt et al. showed that the influence of electrode density seems negligible on the electrochemical performance using HME/DOL.[24] Coin cells were built comparable to the test with DME/DOL. Only the test plan differs in the potential limits because of the absence of $LiNO_3$, which starts undergoing an irreversible reduction reaction at a voltage below 1.8 V vs. Li/Li^+.[35] For the charging step, after reaching the upper potential limit of 2.5 V a constant voltage is applied until a cut-off current of 0.01 C. This procedure should allow an improved conversion to sulfur.[11] The initial discharge capacity of the HSM-electrode was higher than the EL1-electrode (1249 and 1182 mAh $g(S)^{-1}$). A disadvantage of this system is the low ionic conductivity compared to DME/DOL, which generally leads to a poor rate capability.[33]

Research Article
doi.org/10.1002/batt.202400768
Chemistry Europe
European Chemical Societies Publishing

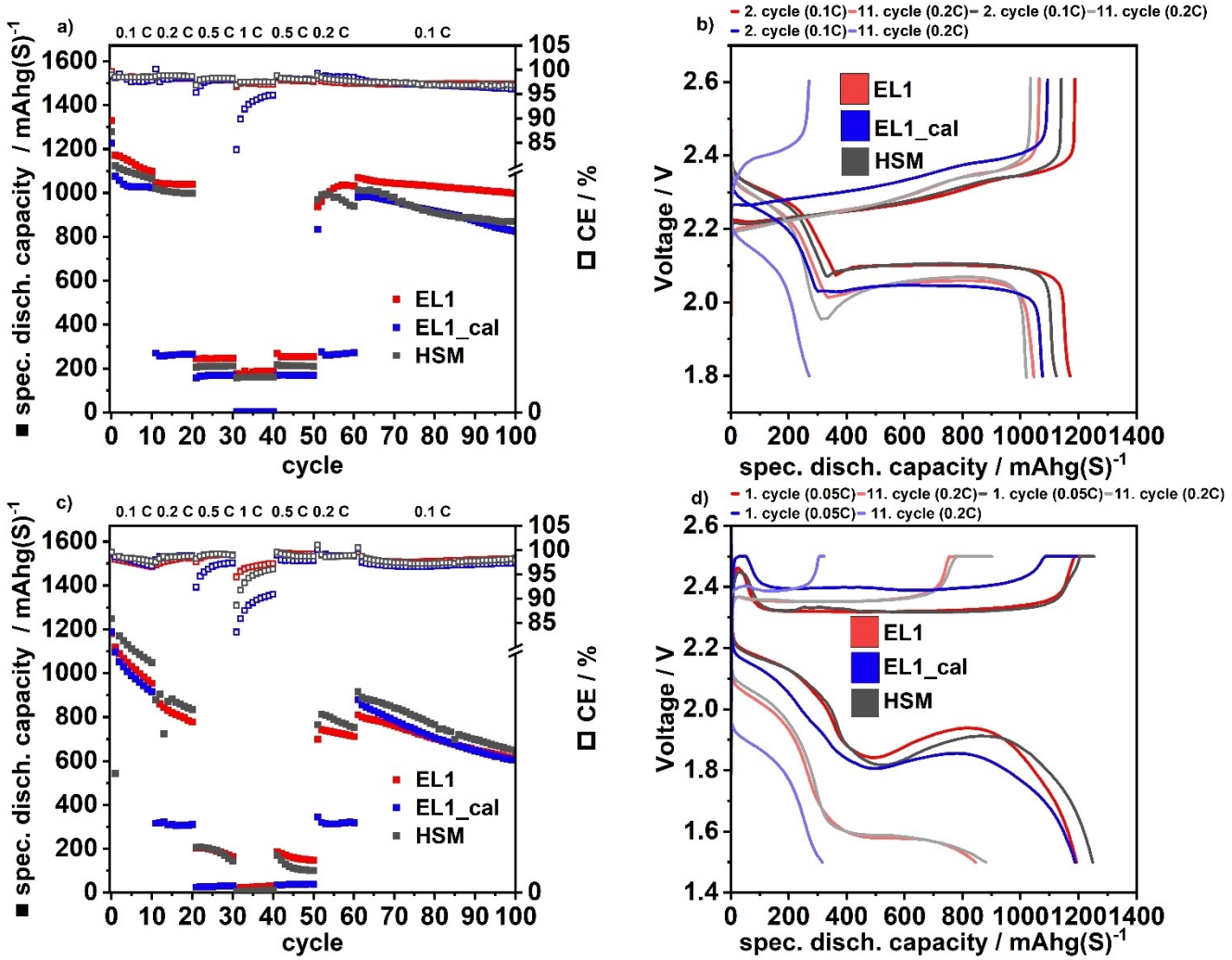

Figure 4. Rate test performance at coin cell level of EL1-electrodes (red: as-prepared; blue: calendered) and HSM-electrodes (grey) with a) DME/DOL electrolyte and b) the corresponding voltage profiles and c) HME/DOL electrolyte and d) the corresponding voltage profiles.

The voltage profiles shown in Figure 4d display a higher capacity gained with the HSM-electrode during the first discharge plateau. As this plateau is linked to the formation of Li_2S_4, more sulfur is addressed by the electrolyte.[11] This is caused by the homogeneity of the HSM-electrode, which is beneficial for the solid-solid mechanism. Increasing the C-rate leads to a higher overpotential and therefore the plateaus are shifted to lower voltages. The constant capacity degradation is related to HME/DOL and its reaction with the Li anode and the constant loss of sulfur by not-transformed Li_2S remaining at the cathode surface after charging.[11] Overall, the higher density of the HSM-electrode has no influence on the performance when HME/DOL is used. This result matches with the findings of Schmidt et al.[24]

Given that the density seems to play a role for DME/DOL electrolyte, and in order to compare the same theoretical porosity for both blending procedures, the EL1-electrode was calendered (EL1_cal) to a density similar to the HSM-electrode. For DME/DOL, the results of the coin cell testing are shown in Figure 4a. The initial capacity of the EL1_cal-electrode drops to 1226 mAh g(S)$^{-1}$. The reason is a lower capacity gain after the first discharge plateau, which is related to less conversion of sulfur to polysulfides. The explanation is the existence of agglomerates, which were stronger compacted than single particles and therefore the electrolyte is not able to reach all the sulfur in this agglomerates anymore. As visible in Figure 4b, the overpotential of the EL1_cal-electrode is higher compared to the HSM-electrode (about 0.07 V). This leads to the effect that at a C-rate of 0.2 C, the potential after the first plateau undercuts the lower voltage limit and therefore the conversion reaction is stopped. For further characterization, electrochemical impedance spectroscopy (EIS) of the three electrodes was measured after assembling coin cells and after running them for 25 cycles. It is shown that the size of semicircles, standing for the inner charge transfer resistance, of the HSM-cell are the smallest compared to the cells with calendered and uncalendered EL1-electrodes. Additionally, cycling of the HSM-cell does not change the resistance, while the cell with calendered EL1-electrode shows an increase. The graphs are shown in Figure S4 and the equivalent circuit model as well as the values for the

Research Article
doi.org/10.1002/batt.202400768
Chemistry Europe
European Chemical Societies Publishing

charge transfer resistances are presented in Table S2. By improving the dispersion of the suspension via HSM-blending, an enhanced rate capability for comparable porosities could be realized. Using HME/DOL electrolyte, the initial capacity of the EL1_cal-electrode remains similar to the uncalendered one (Figure 4c). When discharging with 0.2 C, the capacity of the EL1_cal-electrode drops to around 300 mAh g(S)$^{-1}$. The reason is an increased overpotential as shown in Figure 4d. It is also observable at 0.05 C, but at 0.2 C, the potential undercuts the lower voltage limit. Regarding the charging curves, the overpotential becomes also strongly visible. This phenomenon can be explained by the dispersion of the particles. As mentioned before, agglomerates are existing inside the EL1-electrode, which are strongly compacted leading to a hindered conversion reaction. In addition, the adhesion of the cathode film on the current collector is improved by the HSM-based processing leading to an increased active material utilization. This highlights again the advantages of high dispersion using the HSM.

Electrochemical Performance in Pouch Cells

Coin cells are an appropriate instrument to characterize electrochemical systems, but for testing under practical conditions, it is necessary to use setups realizing lower electrolyte volumes and a defined stack pressure.[10]

For this purpose, pouch cells with five double-sided cathodes were built and tested evaluating the electrode performance under lean electrolyte condition. By symmetrical galvanostatic cycling at 0.1 C, the capacity retention over cycle number was investigated. An external pressure of 0.31 MPa was applied to realize good contacting between the electrodes and to overcome the problem of volume expansion while discharging as well as to stabilize the Li anode.[36] First, an E:S ratio of 4.5 µl mg(S)$^{-1}$ was chosen to fill completely all pores of the carbon matrix and the separator as shown in Table 2. For calculating these theoretical values, the assumption was taken that only separators and electrodes are providing free volume and there are no additional voids inside the pouch cell. The equations can be found in the supporting information as well as the parameters for the calculation, shown in Table S3. The pouch cells tested with DME/DOL electrolyte show a similar behavior in the first cycles as shown in Figure 5a. By using a relative high amount of electrolyte and a low C-rate of 0.1 C, the higher porosity of the EL1-electrode does not influence the capacity retention. Contrary to the coin cell results, the HSM-electrode is providing a similar capacity in this test despite the lower porosity. The voltage profiles for the charging and discharging process at 0.05 C, shown in Figure S5, are comparable and until cycle 25, only a negligible higher overpotential of the HSM-electrode can be observed. After 25 cycles, the degradation of the EL1-cell becomes observable, though. The capacity curve of the HSM-cell remains stable over 30 cycles. The EL1-cell was stopped after 70 cycles, while with HSM-electrodes 90 cycles were reached.

The pouch cells assembled with HME/DOL electrolyte can be cycled for more than 100 times. A disadvantage is the steady loss of capacity. This results from, as described above, the

Table 2. Theoretical proportion of the electrolyte to pore volume for the different electrodes in a multi-layered pouch cell.

	EL 1 (density: 0.35 g cm^{-3})	EL 1_cal (density: 0.5 g cm^{-3})	HSM (density: 0.5 g cm^{-3})
E:S: 4.5 µl mg^{-1}	108%	165%	165%
E:S: 3.0 µl mg^{-1}	72%	110%	110%

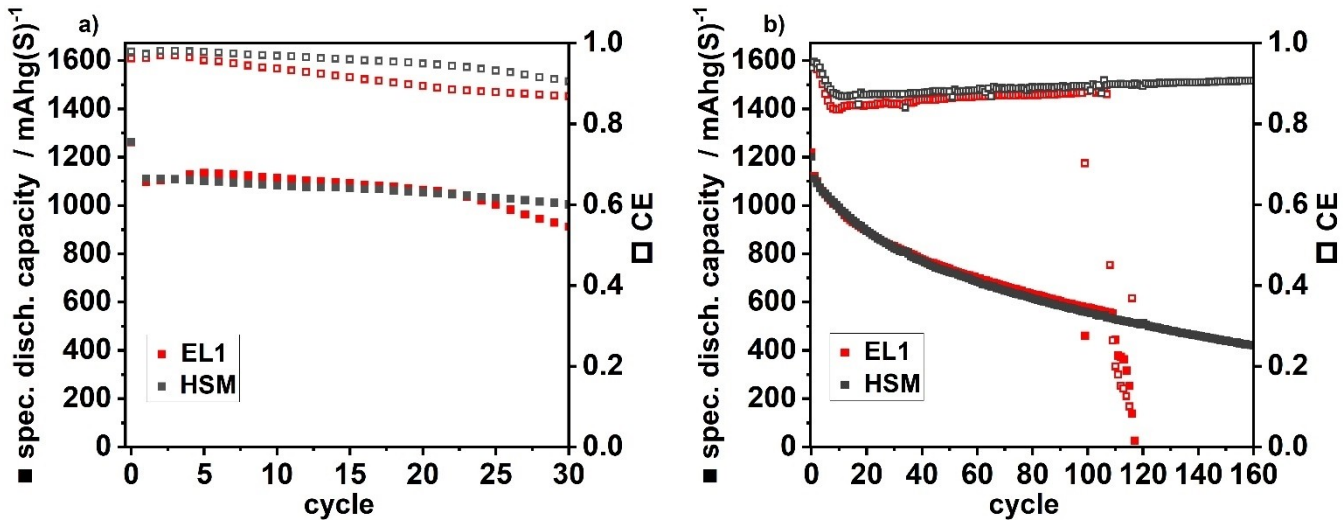

Figure 5. Galvanostatic cycling performance of multi-layered pouch cells with a) DME/DOL and b) HME/DOL electrolyte and an E:S ratio of 4.5 µl mg(S)$^{-1}$ at C/10.

depletion of the HME/DOL electrolyte on the anode side and the agglomeration of Li_2S after discharge and the pore blocking effect provoked by this.[11] The capacity curves of both pouch cells behave similarly as shown in Figure 5b. The degradation of the EL1-cell starts at 110 cycles, while the HSM-cell can be charged and discharged for more than 160 times.

Further, multi-layered pouch cells were built with a lower E:S ratio of 3.0 µl mg(S)$^{-1}$ to clarify the influence of the electrode porosity on the cycle life of the cell. In Figure 6a, the results for the test with DME/DOL electrolyte are displayed. The initial discharge capacities of both cells are comparable (EL1: 1282; HSM: 1300 mAh g(S)$^{-1}$). In the beginning, the same amount of sulfur is converted into polysulfides and then into Li_2S as displayed in the discharge curves in Figure S6. The capacity of the EL1-cell starts to decreases strongly after five cycles while the HSM-cell degrades less severe. The voltage profile of the EL1-cell shows a shorter first discharge plateau after 10 cycles and also a shortened second discharge plateau. Additionally, the overpotential is raising indicating higher inner resistances. For the HSM-electrode, the overpotential raises slowly. The shortening effect of the first discharge plateau starts after 20 cycles. At this cycle number, nearly no polysulfides are converted into Li_2S within the EL1-cell displayed by the absence of the second voltage plateau. Both cells were stopped after 35 cycles not provoking short circuits because the capacity decay of the HSM-cell became stronger and the CE went down fast. The consumption of electrolyte components by reductive decomposition at the anode interface becomes a dominating degradation mechanism in Li–S-cells.[37] This may lead to an increase of polysulfide concentration in the electrolyte and therefore a precipitation of solid reaction products.[38,39] Additionally, the viscosity of the electrolyte is increased as more PS are dissolved causing a lowered Li ion transport.[38] In consequence, the conversion reaction of PS remains incomplete, which becomes visible in an shortened second discharge plateau.[38] However, the main failure is expected from incomplete wetting of the cathode caused by decomposition of electrolyte in gaseous products or interlayers onside both electrodes.[40] Additional voids created by porous grown Li intensifies this effect.[41,42] By providing low electrolyte excess, this phenomenon is particularly promoted. Lowering the cathode porosity can decelerate this effect and thus leading to longer cycle life.

The pouch cells with HME/DOL electrolyte and a low E:S ratio of 3.0 µl mg(S)$^{-1}$ behave comparably to the cells with a E:S ratio of 4.5, but the end of lifetime is reached earlier and there is a higher overpotential observable for the cells with lower electrolyte amount, as displayed in Figure S7. The EL1-cell fails after 30 and the HSM-cell after 60 cycles as shown in Figure 6b. The main degradation mechanism is, as described above, the incomplete wetting caused by the electrolyte decomposition leading to an enhanced cycle life for the HSM-cell with its lower cathode porosity. Due to the constant loss of active material by formation of not addressable Li_2S agglomerates during every discharge step,[11] the consumption of electrolyte components is not as significant as with DME/DOL. Further, the decreasing sulfur utilization leads to a lower stress for Li anode resulting in less dendritic growth and consequently, less voids are formed providing additional space for the electrolyte. These effects promote a longer cycle life in HME/DOL, which can be seen for both E:S ratios.

Conclusions

In summary, for the first time in literature a study is presented that describes the crucial effects of shearing forces during slurry-based sulfur cathode production and how these shearing forces can be transferred to up-scaling cathode suspension production. The influence of two different blending procedures, one with a higher and one with a lower shear rate, on the morphology of carbon-sulfur cathodes and their electrochem-

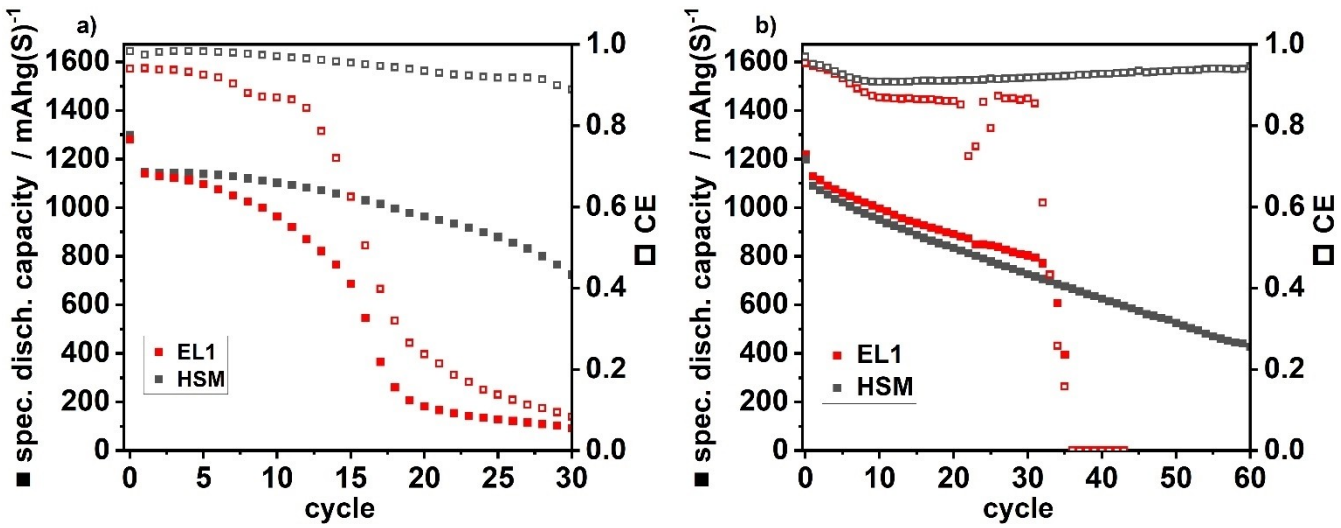

Figure 6. Galvanostatic cycling performance of multi-layered pouch cells with a) DME/DOL and b) HME/DOL electrolyte and an E:S ratio of 3.0 µl mg(S)$^{-1}$ at C/10.

ical behavior were rheologically, structurally and electrochemically investigated in coin cells as well as multi-layered pouch cells, also under lean electrolyte conditions (E:S = 3.0 µl mg-(S)$^{-1}$). It could be shown that by introducing higher shear forces during cathode suspension manufacturing, the cathode adhesion is enhanced and the porosity is reduced leading to slower degradation mechanism caused by electrolyte consumption. Additionally, the dispersion of the cathode composite was enhanced improving the morphological and electrical properties of the electrode. Overall, the cycle life in Li–S pouch cells, both for the reference DME/DOL electrolyte with high PS solubility and HME/DOL as an electrolyte with low PS solubility, was increased by using the HSM-process. These results show the impact of the blender and the possibility of adapting the properties of carbon-sulfur cathodes produced on an industrial scale. In future studies, this blending method could be investigated more by varying parameters to make it possibly suitable for more applications in the field of electrode preparation. Prospectively, this study delivers important findings for overcoming today's challenges in Li–S battery technology.

Experimental Section

Composite Preparation

The pristine sulfur (Sigma Aldrich, > 99 %) and the porous carbon black (Printex XE2-B, Orion Carbon) were blended in a laboratory mixer (EL1, Eirich GmbH). The carbon-to-sulfur ratio was 3/7. Subsequently, the melt infiltration of sulfur was conducted at 155 °C for 30 min under atmospheric conditions. The C–S composite was then blended again in the laboratory mixer with 10.5 wt % MWCNT (NC7000, Nanocyl). In the next step, the composite was ground in an ultra-centrifugal mill (ZM 200, Retsch) with sieve sizes decreasing from 500 to 80 µm.

Electrode Preparation

The C–S composite was used to prepare 500 ml of a water-based suspension on two different ways. For the first one, 146 g of a 1.5 wt % CMC (CMC2200, Daicel) solution was poured in the EL1 and 83 g of the composite and 256 g de-ionized water were added stepwise keeping the solid content of the suspension relatively constant. Finally, 15 g of a SBR suspension (PSBR100, Targray) was also added. The total mixing time was 90 min and a rotation speed between 500 to 1500 min^{-1} were used. For the second preparation procedure, the C–S composite, the CMC solution, the SBR suspension and de-ionized water were given into a container and blended by using a high-shear mixer (HSM, L5 M, Silverson) with a rotation of 9000 min^{-1}. In this case, the mixing time was 10 min. For coating, a roll-to-roll device (Jakob Weiß & Söhne Maschinenfabrik GmbH) was used. The suspension was degassed before casting it on an 8-µm aluminum current collector via using a slot die (FMP). The velocity of band was set to 0.5 m min^{-1} and after the slot die a 2-m convection oven with 70 °C was used to dry the electrodes. The as-prepared electrodes had a sulfur loading of around 2.2 mg cm^{-2}. The final cathode composition was S/PTX/MWCNT/CMC/SBR 60/25/10/2.5/2.5. To increase the electrode density, a part of the cathode sheets were calendered (PCS-30, Jakob Weiß & Söhne Maschinenfabrik GmbH) discontinuously with a fixed pressure of 140 bar.

Structural Characterization of the Composites and Resulting Suspensions

The particle size distribution of the C–S composite after grinding and the as-prepared suspensions was measured with a laser diffraction device (Mastersizer 3000, Malvern Panalytical Ltd). The system allows detecting solids and liquids by two different measurement cells. At least three tests were conducted per sample. The rheological behavior was screened by rotational viscometry using a rheometer (HAAKE Rheostress 1, Thermo Fisher Scientific) with double cone geometry and a test plan with shear rates from 10 to 500 s^{-1}.

Structural Characterization of the Resulting Electrodes

The surface morphology of the electrodes was characterized by laser-scanning microscopy (VK-X 3000, Keyence). The objective provided a 20-fold magnification. For assembling and analyzing the detected images, the software VK-X 3000 MultiFileAnalyzer was used. Additionally, to monitor the swelling behavior of the electrodes, a droplet of 20 µl electrolyte was placed on the surface of the electrode samples. Images of the surface were taken with an objective of 10-fold magnification immediately and after 300/500 s. The surface morphology of the electrodes was also characterized via SEM (JSM-6060, JEOL) with an accelerating voltage of 10 kV. For testing the tensile force, an adhesive tape of 12-mm diameter was pressed with a force of 35 N on a 15-mm diameter sample and then removed with defined speed. The forces were measured using a force gauge (FH50, Sauter). The porosity of both cathodes was measured using Hg intrusion porosimetry. Therefore, a MicroActive AutoPore V9600 (Micromeritics Instrument Corporation) at a temperature of 22.6 °C was used in a pressure range from 0.1 to 61000 psi. The weight of the Al current collector was subtracted from the sample weight.

Electrochemical Characterization

For measuring the composite volume resistivity (CVR), the system RM2610 by Hioki was used. The electrochemical impedance spectroscopy (EIS) was performed by using coin cells built up as described in the following and at a SoC of 100 %. A Biologic VMP3 system and a frequency range of 1 MHz to 1 Hz were used for the measurements. The electrode disks (15-mm diameter) were dried in a vacuum oven for 1.5 h at 50 °C before transferring them into an argon-filled glovebox (MBraun, conditions: < 0.1 ppm O_2 and H_2O). For the coin cells (CR2016) a PE separator (thickness: 12 µm; diameter: 19 mm), a lithium chip (thickness: 250 µm; diameter: 15.6 mm) and a steel spacer (thickness: 10 mm) were used. Two different ether-based electrolytes were used, first a mixture of 1,2-dimethoxyethane (DME) and 1,3-dioxolane (DOL) (v:v 1/1), with 1 M lithium bis(trifluoromethanesulfonyl)imide (LiTFSI) and 0.5 M $LiNO_3$, and second a mixture of hexyl methyl ether (HME) and DOL (v:v 9/1) with 2 M LiTFSI. The electrolyte-to-sulfur ratio (E:S) used for all coin cells was fixed at 7 µl mg(S)$^{-1}$. For the multi-layered pouch cells five double-side coated cathodes, 12 µm PE separator and double-sided Li foil (2×50 µm) were stacked. Principal details for the pouch cell data can be found elsewhere.[9] While cell testing, a constant uniaxial pressure of 0.31 MPa was applied. The electrochemical testing was conducted in a climate chamber with a constant temperature of 25 °C. The galvanostatic cycling measurements were done with a BASYTEC CTS system. The coin cells with DME/DOL-electrolyte were charged with a constant rate of C/10 in a voltage window from 1.8 to 2.6 V vs. Li/Li+. For pouch cells, a window of 1.9 to 2.6 V was used. For the first discharge, a rate of C/20 was applied. The C-rates were calculated based on the theoretical discharge capacity of sulfur with 1672 mAh g^{-1}. The cells with HME/

DOL-electrolyte (voltage range: 1.5–2.5 V vs. Li/Li+) were also charged with C/10, but at the end of charge, a constant voltage step at 2.5 V was applied until a current of 1% of the nominal capacity was reached. The first discharge was conducted with C/20. Except the first discharge, all pouch cells were cycled at 0.1 C using the same voltage limits as for coin cell tests. For evaluation, at least three coin cells and two pouch cells of the same type were built and analyzed.

Acknowledgements

The authors wish to thank Peter Fleischer and Cathleen Tschelzek for pouch cell assembly. This work has received funding from the Federal Ministry of Education and Research, Germany (BMBF), in the project SkaLiS (03XP0398). Open Access funding enabled and organized by Projekt DEAL.

Conflict of Interests

The authors declare no conflict of interest.

Data Availability Statement

The data that support the findings of this study are available from the corresponding author upon reasonable request.

Keywords: Batteries · Cathodes · Lithium · Shear forces · Sulfur

[1] H. D. Yoo, E. Markevich, G. Salitra, D. Sharon, D. Aurbach, *Mater. Today* **2014**, *17*, 110–121.
[2] M. Wild, L. O'Neill, T. Zhang, R. Purkayastha, G. Minton, M. Marinescu, G. J. Offer, *Energy Environ. Sci.* **2015**, *8*, 3477–3494.
[3] A. Fotouhi, D. Auger, L. O'Neill, T. Cleaver, S. Walus, *Energies* **2017**, *10*, 1937.
[4] X.-P. Gao, H.-X. Yang, *Energy Environ. Sci.* **2010**, *3*, 174–189.
[5] L. Borchardt, M. Oschatz, S. Kaskel, *Chemistry* **2016**, *22*, 7324–7351.
[6] Y. Ye, F. Wu, Y. Liu, T. Zhao, J. Qian, Y. Xing, W. Li, J. Huang, L. Li, Q. Huang et al., *Adv. Mater.* **2017**, *29*, 1700598.
[7] Q. Cheng, Z.-X. Chen, X.-Y. Li, L.-P. Hou, C.-X. Bi, X.-Q. Zhang, J.-Q. Huang, B.-Q. Li, *J. Energy Chem.* **2023**, *76*, 181–186.
[8] Z.-X. Chen, L.-P. Hou, C.-X. Bi, Q. Cheng, X.-Q. Zhang, B.-Q. Li, J.-Q. Huang, *Energy Storage Mater.* **2022**, *53*, 315–321.
[9] S. Dörfler, S. Walus, J. Locke, A. Fotouhi, D. J. Auger, N. Shateri, T. Abendroth, P. Härtel, H. Althues, S. Kaskel, *Energy Tech.* **2021**, *9*, 2000694.
[10] S. Dörfler, H. Althues, P. Härtel, T. Abendroth, B. Schumm, S. Kaskel, *Joule* **2020**, *4*, 539–554.
[11] C. Weller, J. Pampel, S. Dörfler, H. Althues, S. Kaskel, *Energy Tech.* **2019**, *7*, 1900625.
[12] L.-L. Su, N. Yao, Z. Li, C.-X. Bi, Z.-X. Chen, X. Chen, B.-Q. Li, X.-Q. Zhang, J.-Q. Huang, *Angew. Chem. Int. Ed.* **2024**, *63*, e202318785.
[13] T. Liu, H. Li, J. Yue, J. Feng, M. Mao, X. Zhu, Y.-S. Hu, H. Li, X. Huang, L. Chen et al., *Angew. Chem. Int. Ed.* **2021**, *60*, 17547–17555.
[14] C. Kensy, D. Leistenschneider, S. Wang, H. Tanaka, S. Dörfler, K. Kaneko, S. Kaskel, *Batteries & Supercaps* **2021**, *4*, 612–622.
[15] J. Wang, J. Yang, J. Xie, N. Xu, *Adv. Mater.* **2002**, *14*, 963–965.
[16] J.-W. Park, S.-C. Jo, M.-J. Kim, I.-H. Choi, B. G. Kim, Y.-J. Lee, H.-Y. Choi, S. Kang, T. Kim, K.-J. Baeg, *NPG Asia Mater.* **2021**, *13*.
[17] C. Yan, X.-Q. Zhang, J.-Q. Huang, Q. Liu, Q. Zhang, *Trends Chem.* **2019**, *1*, 693–704.
[18] W. Chen, Y. Hu, Y. Liu, S. Wang, A. Hu, T. Lei, Y. Li, P. Li, D. Chen, L. Xia et al., *Adv. Mater.* **2024**, *36*, e2312880.
[19] E. Cha, J. H. Yun, D. K. Kim, *APL Mater.* **2022**, *10*, 020701.
[20] M. Hagen, D. Hanselmann, K. Ahlbrecht, R. Maça, D. Gerber, J. Tübke, *Adv. Energy Mater.* **2015**, *5*, 1401986.
[21] A. Gröbmeyer, J. Becking, P. M. Bieker, M. Winter, M. C. Stan, *Energy Tech* **2019**, *7*, 1800789.
[22] J. Li, Z. Xiao, X. Zhou, W. Zhang, J. Zhang, Y. Gan, H. Huang, X. He, G. Wang, Y. Xia, *J. Electron. Mater.* **2022**, *51*, 4115–4124.
[23] P. Titscher, P. Schön, M. Horst, U. Krewer, A. Kwade, *Energy Tech* **2018**, *6*, 1139–1147.
[24] F. Schmidt, S. Ehrling, K. Schönherr, S. Dörfler, T. Abendroth, H. Althues, S. Kaskel, *Energy Tech* **2022**, *10*, 2100721.
[25] N. Kang, Y. Lin, L. Yang, D. Lu, J. Xiao, Y. Qi, M. Cai, *Nat. Commun.* **2019**, *10*, 4597.
[26] F. Schmidt, M. Fiedler, T. Arlt, A. De, F. Hoffmann, F. Wilde, S. Dörfler, B. Schumm, T. Abendroth, H. Althues, et al., *Energy Tech* **2023**, *11*, 2300518.
[27] M. H. Pahl, *Mischen und Rühren. Grundlagen und moderne Verfahren*, Wiley-VCH, Weinheim, **2007**.
[28] D. Aurbach, E. Pollak, R. Elazari, G. Salitra, C. S. Kelley, J. Affinito, *J. Electrochem. Soc.* **2009**, *156*, A694.
[29] S. Xiong, K. Xie, Y. Diao, X. Hong, *Electrochim. Acta* **2012**, *83*, 78–86.
[30] N. Ding, L. Zhou, C. Zhou, D. Geng, J. Yang, S. W. Chien, Z. Liu, M.-F. Ng, A. Yu, T. S. A. Hor, et al., *Sci. Rep.* **2016**, *6*, 33154.
[31] S. S. Zhang, *J. Power Sources* **2016**, *322*, 99–105.
[32] F. Schmidt, A. Korzhenko, P. Härtel, F. S. Reuter, S. Ehrling, S. Dörfler, T. Abendroth, H. Althues, S. Kaskel, *JPhys Energy* **2022**, *4*, 14004.
[33] T. Boenke, S. Kirchhoff, F. S. Reuter, F. Schmidt, C. Weller, S. Dörfler, K. Schwedtmann, P. Härtel, T. Abendroth, H. Althues, et al., *Nano Res.* **2023**, *16*, 8313–8320.
[34] C. Kensy, *Dissertation*, Technische Universität Dresden, Dresden, **2022**.
[35] S. S. Zhang, *J. Electrochem. Soc.* **2012**, *159*, A920–A923.
[36] P. R. Chinnam, L. Xu, L. Cai, N. L. Cordes, S. Kim, C. M. Efaw, D. J. Murray, E. J. Dufek, H. Xu, B. Li, *Adv. Energy Mater.* **2022**, *12*, 2103048 .
[37] L. Shi, S.-M. Bak, Z. Shadike, C. Wang, C. Niu, P. Northrup, H. Lee, A. Y. Baranovskiy, C. S. Anderson, J. Qin, et al., *Energy Environ. Sci.* **2020**, *13*, 3620–3632.
[38] J. Guo, J. Li, H. Liu, S. Li, F. Qin, B. Hong, *Ionics* **2021**, *27*, 3347–3356.
[39] M. Zhao, B.-Q. Li, H.-J. Peng, H. Yuan, J.-Y. Wei, J.-Q. Huang, *Angew. Chem. Int. Ed.* **2020**, *59*, 12636–12652.
[40] W. Zhang, S. Li, A. Zhou, H. Song, Z. Cui, L. Du, *Molecules* **2021**, *26*, 6341 .
[41] O. Leonet, I. Landa-Medrano, A. Shafique, S. Yari, V. Rangasamy, A. Vanhulsel, M. Safari, M. K. van Bael, an Hardy, I. Urdampilleta et al., *Electrochim. Acta* **2023**, *464*, 142889.
[42] R. Weber, J.-H. Cheng, A. J. Louli, M. Coon, S. Hy, J. R. Dahn, *J. Electrochem. Soc.* **2019**, *166*, A3250–A3253.

Manuscript received: December 5, 2024
Revised manuscript received: February 20, 2025
Accepted manuscript online: February 24, 2025
Version of record online: March 6, 2025